RESEARCH ARTICLE | MAY 15 1998

Minimization of ion micromotion in a Paul trap

D. J. Berkeland; J. D. Miller; J. C. Bergquist; W. M. Itano; D. J. Wineland

J. Appl. Phys. 83, 5025–5033 (1998)
https://doi.org/10.1063/1.367318

Minimization of ion micromotion in a Paul trap

D. J. Berkeland,[a] J. D. Miller,[b] J. C. Bergquist, W. M. Itano, and D. J. Wineland
National Institute of Standards and Technology, 325 Broadway, Boulder, Colorado 80303

(Received 26 November 1997; accepted for publication 12 February 1998)

Micromotion of ions in Paul traps has several adverse effects, including alterations of atomic transition line shapes, significant second-order Doppler shifts in high-accuracy studies, and limited confinement time in the absence of cooling. The ac electric field that causes the micromotion may also induce significant Stark shifts in atomic transitions. We describe three methods of detecting micromotion. The first relies on the change of the average ion position as the trap potentials are changed. The second monitors the amplitude of the sidebands of a narrow atomic transition, caused by the first-order Doppler shift due to the micromotion. The last technique detects the Doppler shift induced modulation of the fluorescence rate of a broad atomic transition. We discuss the detection sensitivity of each method to Doppler and Stark shifts, and show experimental results using the last technique. [S0021-8979(98)05610-2]

I. INTRODUCTION

Because of their low velocities, cooled and confined ions can provide the basis for accurate and stable frequency standards and atomic clocks. For example, for $^{199}Hg^{+}$ ions trapped in an rf Paul trap and laser cooled to the Doppler limit, the magnitude of the fractional second-order Doppler (time dilation) shift of transition frequencies can be as low as 2×10^{-18}.[1] However, due to the ion motion synchronous with the trap ac field (the ''micromotion''), this shift can be orders of magnitude larger if the average ion position is not at the nodal position of the trap's ac electric field. To realize the high accuracy of a trapped-ion frequency standard, the ion micromotion must be minimized. In this article, we discuss ion micromotion in a Paul trap and its associated effects on stored ions and their transition frequencies. We also describe methods to detect and minimize micromotion, and present experimental data using one of these methods.

II. MICROMOTION IN A PAUL TRAP

For brevity, we characterize motion of a single ion in one type of Paul trap that may be particularly useful for high-accuracy spectroscopy. The results in this section can be generalized to other types of Paul traps. If several ions are stored in the same trap, the equations of motion must be modified to include modes of collective motion. However, the conclusions about micromotion and its effects are still valid.

Figure 1 shows a schematic diagram of a linear Paul trap.[1–7] Electrodes 1 and 3 are held at ground potential, while the potential of electrodes 2 and 4 is $V_0\cos(\Omega t)$. Typically, for atomic ions, $\Omega/2\pi>100$ kHz and $|V_0|<1000$ V. Near the axis of the trap the potential due to the electrodes is

$$V(x,y,t)=\frac{V_0}{2}\left(1+\frac{x^2-y^2}{R'^2}\right)\cos(\Omega t). \tag{1}$$

R is the perpendicular distance from the trap axis to the trap electrodes [shown in Fig. 1(b)], and $R'\cong R$ ($R'=R$ if the trap electrodes are hyperbolic cylinders of infinite length).[2,3] The gradient of the corresponding electric field confines the ion radially in a harmonic pseudopotential.[8] To confine the ion axially, two endcaps held at potential U_0 create a static potential $U(x,y,z)$. Near the center of the trap, $U(x,y,z)$ can be approximated by

$$U(x,y,z)=\frac{\kappa U_0}{Z_0^2}\left[z^2-\tfrac{1}{2}\,(x^2+y^2)\right], \tag{2}$$

where $\kappa(<1)$ is a geometrical factor and Z_0 is shown in Fig. 1(a). Here, for simplicity, we have neglected the (small) component of alternating electric field along the z axis caused by the electrode configuration shown in Fig. 1. Linear trap electrode geometries which eliminate this field are discussed in Refs. 1 and 2 (see also Sec. V). From Eqs. (1) and (2), the total electric field is

$$\mathbf{E}(x,y,z,t)=-V_0\left(\frac{x\hat{x}-y\hat{y}}{R'^2}\right)\cos(\Omega t) - \frac{\kappa U_0}{Z_0^2}\left[2z\hat{z}-x\hat{x}-y\hat{y}\right]. \tag{3}$$

The equations of motion for a single ion of mass m and charge Q in the above field are given by the Mathieu equation

$$\ddot{u}_i+\left[a_i+2q_i\cos(\Omega t)\right]\frac{\Omega^2}{4}\,u_i=0, \tag{4}$$

where $\mathbf{u}=u_x\hat{x}+u_y\hat{y}+u_z\hat{z}$ is the position of the ion using the coordinate system shown in Fig. 1(b), and from Eq. (3),

$$a_x=a_y=-\frac{1}{2}\,a_z=-\frac{4Q\kappa U_0}{mZ_0^2\Omega^2}, \tag{5}$$

and

$$q_x=-q_y=\frac{2QV_0}{mR'^2\Omega^2},\quad q_z=0. \tag{6}$$

[a]Electronic mail: dana.berkeland@boulder.nist.gov
[b]Present address: KLA, Austin, TX.

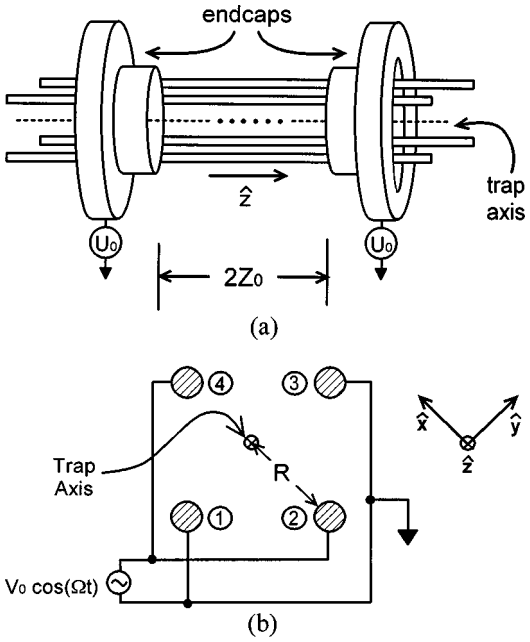

FIG. 1. Linear Paul trap (a) side view and (b) axial view. A string of trapped ions is shown schematically in (a). For clarity, the endcaps are not shown in (b). The trap electrodes are labeled 1, 2, 3, and 4. The trap axis defines the z-axis, and the origin of the z axis is centered between the two endcaps.

For convenience, we also define the unit vectors

$$\hat{u}_x=\hat{x}, \quad \hat{u}_y=\hat{y}, \quad \text{and } \hat{u}_z=\hat{z}. \tag{7}$$

In the typical case where $|q_i|\ll 1$ and $|a_i|\ll 1$, the first-order solution to Eq. (4) is[9]

$$u_i(t)\approx u_{1i}\cos(\omega_i t+\varphi_{Si})\left[1+\frac{q_i}{2}\cos(\Omega t)\right], \tag{8}$$

where

$$\omega_i\cong\tfrac{1}{2}\Omega\sqrt{a_i+\tfrac{1}{2}q_i^2} \tag{9}$$

and φ_{Si} is a phase determined by the initial conditions of the ion position and velocity. The ''secular'' motion of the ion is the harmonic oscillation at frequency ω_i and amplitude u_{1i}. The motion corresponding to the $\cos(\Omega t)$ term is driven by the applied ac field, and is called ''micromotion.''

From Eq. (8), the kinetic energy of the ion averaged over a period of the secular motion is

$$E_{Ki}=\tfrac{1}{2}m\langle\dot{u}_i^2\rangle\cong\tfrac{1}{4}mu_{1i}^2(\omega_i^2+\tfrac{1}{8}q_i^2\Omega^2)$$
$$\cong\tfrac{1}{4}mu_{1i}^2\omega_i^2\left(1+\frac{q_i^2}{q_i^2+2a_i}\right), \tag{10}$$

where the first term in the last two expressions is the kinetic energy due to the secular motion, and the second term is the kinetic energy due to the micromotion. For motion parallel to the trap axis, $q_z^2=0$, so the average kinetic energy is due entirely to secular motion. Because the secular motion is typically thermal, incoherent motion, the kinetic energy due to motion in the z direction is

$$E_{Kz}=\tfrac{1}{2}k_BT_z\cong\tfrac{1}{4}mu_{1z}^2\omega_z^2, \tag{11}$$

where k_B is the Boltzmann constant, and the kinetic energy is characterized by a temperature T_z. Typically, in the radial direction, $|a_i|\ll q_i^2(i=x,y)$. The energy of the radial secular motion is then approximately equal to that of the radial micromotion. In this case,

$$E_{Ki}=k_BT_i\cong\tfrac{1}{2}mu_{1i}^2\omega_i^2(i=x,y). \tag{12}$$

The energy of the secular motion can be reduced by cooling.[10] As the amplitude u_{1i} of the secular motion is reduced, the micromotion and its corresponding energy are also reduced according to Eqs. (8) and (10). The Doppler-cooling limit of the ion temperature due to secular motion in one direction is[10]

$$T_D\cong\frac{\hbar\gamma}{2k_B}, \tag{13}$$

where γ is the linewidth of the cooling transition. As an example, for the $^{199}Hg^+$ $5d^{10}6s\ ^2S_{1/2}\rightarrow 5d^{10}6p\ ^2P_{1/2}$ transition used for laser cooling, $\gamma=2\pi\cdot 70$ MHz. The Doppler-limited cooling temperature is $T_D\cong 1.7$ mK.

If, in addition to the trap fields described above, the ion is also subjected to a uniform static electric field $\mathbf{E}_{\rm dc}$, Eq. (4) becomes

$$\ddot{u}_i+[a_i+2q_i\cos(\Omega t)]\frac{\Omega^2}{4}u_i=\frac{Q\mathbf{E}_{\rm dc}\cdot\hat{u}_i}{m}. \tag{14}$$

To lowest order in a_i and q_i, the solution to Eq. (14) is

$$u_i(t)\cong[u_{0i}+u_{1i}\cos(\omega_i t+\varphi_{Si})]\left[1+\frac{q_i}{2}\cos(\Omega t)\right], \tag{15}$$

where

$$u_{0i}\cong\frac{4Q\mathbf{E}_{\rm dc}\cdot\hat{u}_i}{m(a_i+\frac{1}{2}q_i^2)\Omega^2}\cong\frac{Q\mathbf{E}_{\rm dc}\cdot\hat{u}_i}{m\omega_i^2}. \tag{16}$$

The field $\mathbf{E}_{\rm dc}$ displaces the average position of the ion to $\mathbf{u}_0=u_{0x}\hat{x}+u_{0y}\hat{y}+u_{0z}\hat{z}$, but does not directly change u_{1i}. The ac electric field at position $\mathbf{u}_0$ causes micromotion of amplitude $\frac{1}{2}u_{0i}q_i$ along $\hat{u}_i$. We will call this ''excess micromotion,'' to distinguish it from the unavoidable micromotion that occurs when the secular motion carries the ion back and forth through the nodal line of the ac field. Unlike secular motion, excess micromotion cannot be significantly reduced by cooling methods because it is driven motion.

Excess micromotion can also be caused by a phase difference $\varphi_{\rm ac}$ between the ac potentials applied to electrodes 2 and 4. For example, in the trap shown in Fig. 1, the potential applied to the electrode 4 may be $+V_0\cos(\Omega t+\frac{1}{2}\varphi_{\rm ac})$, and to electrode 2, $V_0\cos(\Omega t-\frac{1}{2}\varphi_{\rm ac})$. If $\varphi_{\rm ac}\ll 1$, these potentials are approximately equal to $V_0\cos(\Omega t)-\frac{1}{2}V_0\varphi_{\rm ac}\sin(\Omega t)$ and $V_0\cos(\Omega t)+\frac{1}{2}V_0\varphi_{\rm ac}\sin(\Omega t)$, respectively. Near the trap axis, the additional field due to the $\pm\frac{1}{2}V_0\varphi_{\rm ac}\sin(\Omega t)$ terms is approximately that of two parallel plates held at potentials $\pm\frac{1}{2}V_0\varphi_{\rm ac}\sin(\Omega t)$ and separated by $2R/\alpha$.[11] The value of α depends on the geometry of the trap. We use the method of van Wijngaarden and Drake[12] to calculate the dipole moment for our trap ($R=0.81$ mm, electrode radius $r=0.38$ mm), and find $\alpha=0.75$. If we include a uniform static field, the total electric field near the center of the trap is

$$\mathbf{E}(x,y,z,t)\cong -\frac{V_0}{R'^2}(x\hat{x}-y\hat{y})\cos(\Omega t)-\frac{\kappa U_0}{Z_0^2}\times(2z\hat{z}-x\hat{x}-y\hat{y})+\mathbf{E}_{\rm dc}+\frac{V_0\varphi_{\rm ac}\alpha}{2R}\sin(\Omega t)\hat{x}. \quad (17)$$

With the additional oscillating electric field due to $\varphi_{\rm ac}$, the equations of motion in the y and z directions remain unchanged from Eq. (15). However, if we solve the equation of motion in the x direction to lowest order in a_x, q_x and $\varphi_{\rm ac}$, and use $R'=R$ in Eq. (6), then

$$u_x(t)\cong[u_{0x}+u_{1x}\cos(\omega_{xt}+\varphi_{Sx})][1+\tfrac{1}{2}q_x\cos(\Omega t)]-\tfrac{1}{4}q_xR\alpha\varphi_{\rm ac}\sin(\Omega t). \quad (18)$$

Equation (18) shows that unless $\varphi_{\rm ac}=0$, the excess micromotion in the x direction will not vanish for any average ion position $\mathbf{u}_0$.

From Eqs. (15), (16), and (18), the average kinetic energy due to motion along $\hat{u}_i$ is

$$E_{Ki}\cong\tfrac{1}{4}mu_{1i}^2(\omega_i^2+\tfrac{1}{8}q_i^2\Omega^2)+\frac{4}{m}\left(\frac{Qq_i\mathbf{E}_{\rm dc}\cdot\hat{u}_i}{(2a_i+q_i^2)\Omega}\right)^2+\tfrac{1}{64}m(q_xR\alpha\varphi_{\rm ac}\Omega)^2\delta_{i,x}. \quad (19)$$

In order to compare the size of the last two terms relative to the first, it is useful to write them as $k_BT_{\mu i}/2$, where $T_{\mu i}$ is the equivalent (pseudo) temperature for the kinetic energy due to the excess micromotion along $\hat{u}_i$. A uniform static field along the axial direction does not change E_{Kz}, since it only shifts the position of the minimum of the static potential $U(x,y,z)$. For a $^{199}Hg^+$ ion in a trap with $|a_i|\ll q_i^2\ll 1$ and $\omega_x=2\pi\cdot 100$ kHz, a 1 V mm^{-1} uniform field along the x direction increases $T_{\mu x}$ by 1.4×10^4 K. For $R=1.0$ mm and $\alpha=0.75$, a phase shift of $\varphi_{\rm ac}=1°$ between the trap electrode potentials increases $T_{\mu x}$ by 0.41 K. These effective temperatures are orders of magnitude greater than the 1.7 mK temperature associated with the secular motion at the Doppler-cooling limit.

These phase shifts and electric fields may be reasonably expected. A phase shift can be caused by asymmetries in the electrical impedances of the electrodes. For example, a phase shift will occur if the leads to the trap electrodes have different inductances due to different lengths or geometrical arrangements. A uniform electric field of magnitude 1 V mm^{-1} may develop in a millimeter-sized trap in several ways. Often, an effusive oven located on one side of the trap is used with an electron-emitting filament to produce ions inside the trap. In this case, the trap electrodes may become unevenly coated with the oven contents, which could cause contact potentials of a fraction of a volt. Additionally, the trap electrodes may become unevenly charged when this coating or other dielectric or oxide layer is charged by the emitted electrons. Finally, patch effects due to different crystal planes at the surface of the electrodes also can produce surface potential variations of roughly 100 mV. Although the magnitude of stray fields caused by patch effects and charging of the trap electrodes can be reduced by heating the trap electrodes *in situ*,[13] no technique can eliminate these fields.

Below, we will give general expressions for the effects of excess micromotion and several methods to detect it. To provide examples, we consider the Doppler shifts and the ac Stark shift of the $^{199}Hg^+$ $5d^{10}6s\ ^2S_{1/2}\rightarrow 5d^96s^2\ ^2D_{5/2}$ electric quadrupole transition at 282 nm, and the sensitivity of the various methods used to detect these shifts. Because effects from excess micromotion are negligible in the limit that $|a_i|\gg q_i^2$, in the following sections all examples assume that $|a_i|\ll q_i^2\ll 1$ $(i=x,y)$. We take the physical trap parameters as $R'\approx R=1.0$ mm, $\alpha=0.75$, $\Omega=2\pi\cdot 10$ MHz, $\omega_x\approx\omega_y=2\pi\cdot 1.0$ MHz, and $q_x\approx q_y=0.28$.

III. EFFECTS OF EXCESS ION MICROMOTION

The first-order Doppler shift due to excess micromotion can significantly alter the excitation spectrum of an atomic transition. The spectrum can even change so that a laser heats the ions at frequencies where laser cooling is normally expected.[14,15] Assume that the electric field of the laser used to excite the ion has amplitude $\mathbf{E}_0$, frequency $\omega_{\rm laser}$, phase $\varphi_{\rm laser}$, and wave vector $\mathbf{k}$. From Eqs. (15) and (18), in the rest frame of an ion undergoing excess micromotion, this laser field becomes

$$\mathbf{E}(t)=\mathrm{Re}\{\mathbf{E}_0\exp[i\mathbf{k}\cdot\mathbf{u}-i\omega_{\rm laser}t+\varphi_{\rm laser}]\}\cong\mathrm{Re}\{\mathbf{E}_0\exp[i\mathbf{k}\cdot(\mathbf{u}_0+\mathbf{u}')-i\omega_{\rm laser}t+\varphi_{\rm laser}]\}, \quad (20)$$

where $\mathbf{u}'$ is the amplitude of the excess micromotion. To isolate the effect of excess micromotion, we have assumed that $|u_{0i}|\gg|u_{1i}|$ and $|R\alpha\varphi_{\rm ac}|\gg|u_{1i}|$. From Eqs. (15) and (18),

$$\mathbf{k}\cdot\mathbf{u}'(t)=\beta\Omega\cos(\Omega t+\delta), \quad (21)$$

where

$$\beta=\sqrt{\left(\frac{1}{2}\sum_{i=x,y}k_iu_{0i}q_i\right)^2+\left(\frac{1}{4}k_xq_xR\alpha\varphi_{\rm ac}\right)^2}, \quad (22)$$

$$\sin\delta=\frac{k_xq_xR\alpha\varphi_{\rm ac}}{\sqrt{(2\Sigma_{i=x,y}k_iu_{0i}q_i)^2+(k_xq_xR\alpha\varphi_{\rm ac})^2}}, \quad (23)$$

and

$$\cos\delta=\frac{2\Sigma_{i=x,y}k_iu_{0i}q_i}{\sqrt{(2\Sigma_{i=x,y}k_iu_{0i}q_i)^2+(k_xq_xR\alpha\varphi_{\rm ac})^2}}. \quad (24)$$

With the Bessel function expansion

$$\exp[i\beta\cos(\Omega t+\delta)]=\sum_{n=-\infty}^{\infty}J_n(\beta)\exp[in(\Omega t+\delta+\pi/2)], \quad (25)$$

Eq. (20) can be written as

$$\mathbf{E}(t)=\mathrm{Re}\left\{\mathbf{E}_0\exp[i\mathbf{k}\cdot\mathbf{u}_0]\sum_{n=-\infty}^{\infty}J_n(\beta)\times\exp[-i\omega_{\rm laser}t+\varphi_{\rm laser}+in(\Omega t+\delta+\pi/2)]\right\}. \quad (26)$$

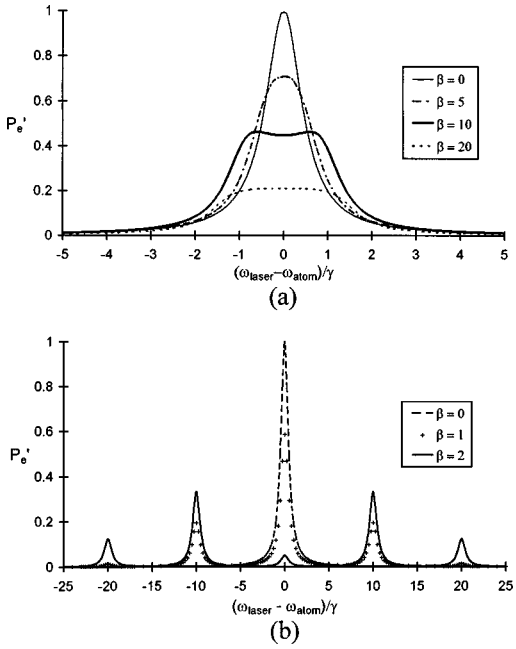

FIG. 2. Effect of micromotion on the spectrum of P_e (excited state population). We plot $P_e'=P_e[\hbar\gamma/(2\mathscr{P}|E_0|)]^2$ for various values of β. For both graphs, we assume that the ion is driven below the saturation limit. (a) $\Omega/\gamma=0.1$. For $\beta=10$, heating occurs in the regions $<0.6<(\omega_{\text{laser}}-\omega_{\text{atom}})/\gamma<0$ and $(\omega_{\text{laser}}-\omega_{\text{atom}})/\gamma>0.6$. (b) $\Omega/\gamma=10$. For $\beta>0$, heating can occur when the laser frequency is tuned near, but above the center of, any of the sideband frequencies.

We define $\mathscr{P}|\mathbf{E}|$ as the amplitude of the interaction matrix element between atomic levels $|e\rangle$ and $|g\rangle$ coupled by an electric field $\text{Re}\{\mathbf{E}e^{i\omega+i\varphi}\}$. Here, ω is the field frequency and φ is the field phase. If the field of Eq. (26) interacts with the atom in the low intensity limit

$$\frac{\mathscr{P}|\mathbf{E}_0|}{\hbar}\ll\gamma, \tag{27}$$

then the steady-state solution to the optical Bloch equation for the upper level population P_e is[14,15]

$$P_e=\left(\frac{\mathscr{P}|\mathbf{E}_0|}{\hbar}\right)^2\sum_{n=-\infty}^{\infty}\frac{J_n^2(\beta)}{(\omega_{\text{atom}}-\omega_{\text{laser}}+n\Omega)^2+(\frac{1}{2}\gamma)^2}, \tag{28}$$

where ω_{atom} is the resonance frequency of the atomic transition. Figure 2(a) shows the excitation spectrum calculated from Eq. (28) for various magnitudes of micromotion, for $\Omega\ll\gamma$ and in the low intensity limit. As β increases from 0, the frequency modulation from the excess micromotion first broadens the transition. This decreases the rate at which a laser can cool the ion. For larger values of β, the line shape can develop structure that causes the laser to heat, rather than cool the ion, even when $\omega_{\text{laser}}-\omega_{\text{atom}}<0$. Figure 2(b) shows the effect of micromotion when $\Omega\gg\gamma$. As β increases, the excitation spectrum develops sidebands at $\pm n\Omega$ ($n=1,2,3,...$), and the strength of the carrier transition decreases. Heating now occurs when the laser frequency is tuned near, but above the center frequency of any of the sidebands.

Ion motion also produces a second-order Doppler (time-dilation) shift of atomic transition frequencies

$$\Delta\nu_{D2}=-\frac{E_K}{mc^2}\,\nu=-\frac{1}{2}\frac{\langle V^2\rangle}{\langle c^2\rangle}\,\nu, \tag{29}$$

where ν is the atomic transition frequency and V is the ion velocity. From Eqs. (12) and (19), the fractional shift due to motion along $\hat{u}_i$ can be written as

$$\left(\frac{\Delta\nu_{D2}}{\nu}\right)_i\approx-\frac{1}{mc^2}\left[\frac{k_BT_i(a_i+q_i^2)}{(2a_i+q_i^2)}+\frac{4}{m}\left(\frac{Qq_i\mathbf{E}_{\text{dc}}\cdot\hat{u}_i}{(2a_i+q_i^2)\Omega}\right)^2+\frac{m(q_xR\alpha\varphi_{\text{ac}}\Omega)^2}{64}\,\delta_{i,x}\right]. \tag{30}$$

If $\mathbf{E}_{\text{dc}}=0$, $\varphi_{\text{ac}}=0$ and $T_x=1.7$ mK, motion in the x direction for a $^{199}Hg^+$ ion contributes -8×10^{-19} to the fractional second-order Doppler shift. However, if $\varphi_{\text{ac}}=1°$, the fractional shift becomes -9×10^{-15}. A 1 V mm^{-1} field along the x axis further increases the magnitude of the fractional shift by 3×10^{-14}.

The ac field that causes micromotion can also cause significant ac Stark shifts. The Stark shift due to the field the ion experiences is approximately

$$\Delta\nu_S\cong\sigma_S\langle E(\mathbf{u},t)^2\rangle, \tag{31}$$

where σ_S is the static Stark shift constant and $\langle E(\mathbf{u},t)^2\rangle$ is the time-averaged square of the electric field at the ion position. To lowest order in q_i and a_i, substituting Eq. (18) into Eq. (17) gives

$$\langle E_i^2(\mathbf{u},t)\rangle\cong\frac{m\Omega^2k_BT_i}{2Q^2}\,\frac{a_i^2+2q_i^2}{2a_i+q_i^2}+8\left(\frac{q_i\mathbf{E}_{\text{dc}}\cdot\hat{u}_i}{2a_i+q_i^2}\right)^2+\frac{1}{32}\left(\frac{mq_xR\alpha\varphi_{\text{ac}}\Omega^2}{Q}\right)^2\delta_{i,x}. \tag{32}$$

The second term is much greater than the square of $\mathbf{E}_{\text{dc}}\cdot\hat{u}_i$ when $|a_i|\ll q_i^2\ll1$, so a small uniform static field can induce a large Stark shift.

Stark shifts have been measured for the three Zeeman components of the 1.76 μm $6^2S_{1/2}\rightarrow5^2D_{5/2}$ transition in a single $^{138}Ba^+$ ion.[16] The ion, cooled to about 1 mK, was confined in a spherical Paul trap in which $\Omega=2\pi\cdot26$ MHz and $\omega_z=2\pi\cdot2.6$ MHz. A static electric field was applied along the z direction, and the shift of the transition frequency was measured as a function of the field strength. The measured values of σ_S were on the order of $+10^{-6}$ Hz/(V/m)^2 for each Zeeman component. With these values of σ_S, the fractional Stark shift of the transition frequency in the absence of uniform static electric fields was calculated to be 10^{-17}. A 5 mV potential across the 0.3 mm diameter trap was predicted to cause a fractional shift of $+1.2\times10^{-15}$.

We have estimated the static Stark shift constant σ_S of the 282 nm $^{199}Hg^+$ $5d^{10}6s\ ^2S_{1/2}\rightarrow5d^96s^2\ ^2D_{5/2}$ electric quadrupole transition. First, we calculate the matrix elements between the $5d^{10}6s\ ^2S_{1/2}$ ground state and the closest few states with the $5d^{10}6p$ configuration. This gives $\alpha_S=2.1\times10^{-24}$ cm^3 for the polarizability of the ground state. To estimate the polarizability of the $5d^96s^2\ ^2D_{5/2}$ state, we con-

sider transitions from the $5d^9 6s^2\ ^2D_{5/2}$ state to the various states with the configuration $5d^9 6s 6p$. In the $5d^9 6s 6p$ states, one of the two $6s$ electrons of the $^2D_{5/2}$ state has been excited to a $6p$ state. That transition is qualitatively similar to exciting the single $6s$ electron of the $5d^{10}6s\ ^2S_{1/2}$ state to one of the $5d^{10}6p$ states. Hence we assume that the matrix elements between the $5d^9 6s^2$ states and the $5d^9_{5/2}6s6p$ states are similar to those between the $5d^{10}6s$ and $5d^{10}6p$ states. The center of gravity of the $5d^9 6s^2 \rightarrow 5d^9_{5/2}6s6p$ transitions is about 208 nm. This wavelength is not much longer than that of the first $5d^{10}6s \rightarrow 5d^{10}6p$ transition at 194 nm. Thus we expect that the polarizability α_D of the $^2D_{5/2}$ state is on the order of that of the ground state. Both states will be shifted down in energy by a static electric field, since all electric dipole transitions connect them only to higher-lying states. For the electric quadrupole transition, then, we estimate that $|\sigma_S| \leqslant 1.0\times 10^{-6}$ Hz/(V/m)^2.

This number lets us estimate the magnitude of the Stark shift for the 282 nm quadrupole transition, using the parameters stated earlier. If $\mathbf{E}_{\rm dc}=0$, $\varphi_{\rm ac}=0$, and the ion is cooled to the Doppler limit in the x direction, then the Stark shift of the 282 nm quadrupole transition due to the electric field in the x direction is $|\Delta\nu_S/\nu| \leqslant 1.1\times 10^{-18}$. A 1 V mm^{-1} static field along the x direction causes a fractional Stark shift of $|\Delta\nu_S/\nu| \leqslant 9\times 10^{-14}$. If $\varphi_{\rm ac}=1°$, the magnitude of this shift increases by about 3×10^{-14}.

Under favorable circumstances, the second-order Doppler and ac Stark shifts from excess micromotion can be made to cancel. If we consider only the effects of excess micromotion, we have

$$Q\mathbf{E}(\mathbf{u},t) = m\,\frac{d^2\mathbf{u}'}{dt^2} = m\,\frac{d\mathbf{V}_\mu}{dt}, \tag{33}$$

where $\mathbf{V}_\mu$ is the velocity of the excess micromotion. From Eq. (31), the ac Stark shift can be written as

$$\Delta\nu_S \cong \sigma_S \left(\frac{m\Omega}{Q}\right)^2 \langle V_\mu^2\rangle. \tag{34}$$

Using Eq. (29), we can write the sum of the fractional second-order Doppler and ac Stark shifts as

$$\frac{\Delta\nu_S}{\nu} + \frac{\Delta\nu_{2D}}{\nu} \cong \left[\frac{\sigma_S}{\nu}\left(\frac{m\Omega}{Q}\right)^2 - \frac{1}{2c^2}\right]\langle V_\mu^2\rangle. \tag{35}$$

For $\sigma_S > 0$, it might be possible to make the factor in brackets equal to 0. As an example, for the 282 nm quadrupole transition in $^{199}Hg^+$, if $\sigma_S = 1\times 10^{-6}$ Hz/(V/m)^2, this factor is 0 for $\Omega \cong 2\pi\cdot 8.4$ MHz, close to the condition of the experiment reported in Sec. V.

Finally, if several ions are stored in the same trap, excess micromotion can also increase the magnitude of the secular motion. The micromotion and secular motion of a single ion in a Paul trap are highly decoupled, so excess micromotion will typically not increase the secular motion. However, if two or more ions are in the trap, the energy of the excess micromotion of any ion can be parametrically coupled into the energy of the secular motion of the other ions.[7,14,15,17] Since the micromotion is driven by the ac field, this heating is continuous and can limit the lowest temperature attainable by cooling methods. In the absence of cooling mechanisms, the ions can gain enough energy to leave the trap.

IV. DETECTION OF EXCESS MICROMOTION

Different techniques can be used to detect excess micromotion caused by a uniform static field $\mathbf{E}_{\rm dc}$ or phase difference $\varphi_{\rm ac}$ between the trap electrode potentials. In the first of these methods, which is sensitive to excess micromotion caused by static fields, the time-averaged ion position is monitored as the pseudopotential is raised and lowered.[18] If an imaging system is used to view the ion as it is translated, then the ion position in the plane of observation can be determined to the resolution limit of the optics. Translations can also be detected in any direction by monitoring the distance that a focused laser beam must be translated to maintain the maximum photon scattering rate from the ions. Let Δu_{0i} be the measured translation along $\hat{u}_i$ when the secular frequency is reduced from ω_{i1} to ω_{i2}. From Eqs. (16) and (30) (taking $|a_i| \ll q_i^2 \ll 1$), when the secular frequency is ω_{i1}, the fractional second-order Doppler shift due to excess micromotion along $\hat{u}_i$ is

$$\left(\frac{\Delta\nu_{D2}}{\nu}\right) \cong -\frac{1}{2}\left(\frac{\omega_{i2}^2}{\omega_{i1}^2-\omega_{i2}^2}\,\frac{\Delta u_{0i}\omega_{i1}}{c}\right)^2. \tag{36}$$

From Eqs. (16) and (32), the Stark shift due to the ac field along $\hat{u}_i$ is

$$(\Delta\nu_S)_i \cong \sigma_S\left(\frac{\omega_{i2}^2}{\omega_{i1}^2-\omega_{i2}^2}\,\frac{m\Delta u_{0i}\omega_{i1}\Omega}{Q}\right)^2. \tag{37}$$

As an example of the sizes of the detectable shifts, we assume the same parameters for the trap and ion ($^{199}Hg^+$) as above. We assume also that the ion position changes by $|\Delta u_{0x}| = 25\ \mu$m in the x direction when the pseudopotential is lowered to $\omega_x = 2\pi\cdot 0.5$ MHz. Then the second-order Doppler shift when $\omega_x = 2\pi\cdot 1.0$ MHz is $\Delta\nu_{D2}/\nu \cong -1.5\times 10^{-14}$, and the Stark shift of the electric quadrupole transition is $|\Delta\nu_S/\nu| \leqslant 4\times 10^{-14}$.

This technique can also be used by modulating the pseudopotential (by modulating V_0 at frequency $\omega_{\rm mod} \ll \Omega$) while the ion is located in the waist of a laser beam tuned to a cycling transition (for example, the Doppler-cooling transition). We assume that $|a_i| \ll q_i^2 \ll 1$ and that the modulation is adiabatic, so while the magnitude of the excess micromotion changes, the magnitude of the thermal motion is approximately constant. Suppose that the laser beam has a transverse Gaussian intensity profile

$$I(r) = I_0\ \exp(-2r^2/w_0^2), \tag{38}$$

and that the ion lies on the half-intensity radius of the beam

$$r = r_0 \cong \sqrt{\frac{\ln 2}{2}}\,w_0. \tag{39}$$

The secular frequency is given by

$$\omega_i' = \omega_i + \Delta\omega_i\ \cos(\omega_{\rm mod}t + \varphi_{\rm mod}), \tag{40}$$

where

$$\frac{\Delta\omega_x}{\omega_x}=\frac{\Delta\omega_y}{\omega_y}\cong\frac{\Delta V_0}{V_0}, \tag{41}$$

φ_{mod} is the phase of the modulation, and ΔV_0 is the modulation of the trap rf amplitude. Here, for simplicity, we assume that $\Delta\omega_i/\omega_i\ll 1$. The ion position averaged over a cycle of the rf potential varies as

$$u'_{0i}=u_{0i}-\Delta u_{0i}\,\cos(\omega_{\mathrm{mod}}t+\varphi_{\mathrm{mod}}), \tag{42}$$

where

$$\Delta u_{0i}=\frac{2u_{0i}\Delta V_0}{V_0}\ (i=x,y). \tag{43}$$

We define $\mathbf{r}=r\hat{r}$ as the vector from the laser beam axis to the ion position (such that $\hat{r}\cdot\mathbf{k}=0$). If $\Delta\mathbf{u}_0\cdot\hat{r}\ll w_0$, then the laser intensity in the rest frame of the ion is

$$I\cong I_0\left[\frac{1}{2}-\frac{\sqrt{2\ln 2}\ \Delta\mathbf{u}_0\cdot\hat{r}\ \cos(\omega_{\mathrm{mod}}t+\varphi_{\mathrm{mod}})}{w_0}\right]$$

$$\equiv\tfrac{1}{2}\,I_0-\Delta I\,\cos(\omega_{\mathrm{mod}}t+\varphi_{\mathrm{mod}}). \tag{44}$$

In the low intensity limit, the detected fluorescence signal is $R_d=\frac{1}{2}R_{\max}-\Delta R_d\cos(\omega_{\mathrm{mod}}t+\varphi_{\mathrm{mod}})$. Here, ΔR_d is the amplitude of the signal synchronous with the pseudopotential modulation, and $R_{\max}$ is the signal when the ion is at the center of the laser beam profile. We can write

$$\frac{\Delta R_d}{R_{\max}}=\frac{\Delta I}{I_0}\cong\sqrt{2\ln 2}\,\frac{\Delta\mathbf{u}_0\cdot\hat{r}}{w_0}=\sqrt{2\ln 2}\,\frac{|\Delta u_0|}{w_0}\cos\,\theta_{\mu r}, \tag{45}$$

where $\theta_{\mu r}$ is the angle between $\Delta\mathbf{u}_0$ and $\hat{r}$. From the measured value of $\Delta R_d/R_{\max}$ and for a known value of $\Delta V_0/V_0$, we can determine u_{0i} from Eqs. (43) and (45). From Eqs. (16), (30), and (32), we can then determine the corresponding values of $\Delta\nu_D/\nu$ and $\langle E_i^2\rangle$, analogous to Eqs. (36) and (37). Generally, $\cos\theta_{\mu r}$ is not known, but it can be maximized and the direction of $\Delta\mathbf{u}$ can be determined by moving the laser beam appropriately.

The main disadvantage to the above techniques is that they are not sensitive to excess micromotion caused by a phase shift φ_{ac} between the potentials applied to the trap electrodes. If $u_{0x}=0$ but $\varphi_{\mathrm{ac}}\neq 0$, the average ion position will not change as the pseudopotential is raised and lowered, as indicated in Eq. (18). Techniques that sense the magnitude of the first-order Doppler shift caused by the excess micromotion eliminate this problem.

We will assume that we measure the effects of the first-order Doppler shift on an optical transition with natural width γ. Previously, first-order Doppler shifts of microwave spectra have been used to determine the temperature of the secular motion of trapped ions.[19,20] We first take the case in which $\Omega\gg\gamma$. The micromotion can be monitored by measuring the scattering rate R_0 when the laser is tuned to the carrier ($\omega_{\mathrm{laser}}-\omega_{\mathrm{atom}}=0$) and R_1 when tuned to the first sideband ($\omega_{\mathrm{laser}}-\omega_{\mathrm{atom}}=\pm\Omega$)[21] [see Fig. 2(b)]. From Eq. (28), in the low intensity limit,

$$\frac{R_1}{R_0}=\frac{J_1^2(\beta)}{J_0^2(\beta)}, \tag{46}$$

where β is defined in Eq. (22). For $\beta\ll 1$,

$$\frac{R_1}{R_0}\cong(\tfrac{1}{2}\beta)^2, \tag{47}$$

and since

$$\beta=|\mathbf{k}\cdot\mathbf{u}'|=\left|\frac{\mathbf{k}\cdot\mathbf{V}_\mu}{\Omega}\right|, \tag{48}$$

the fractional second-order Doppler shift can be written as

$$\frac{\Delta\nu_{D2}}{\nu}\cong-\left(\frac{\Omega}{ck\,\cos\,\theta_{\mu k}}\right)^2\frac{R_1}{R_0}, \tag{49}$$

where $\theta_{\mu k}$ is the angle between $\hat{k}$ and the direction of the excess micromotion. From Eqs. (34), (47), and (48), the corresponding Stark shift can be written

$$\Delta\nu_S\cong 2\sigma_S\left(\frac{m\Omega^2}{Qk\,\cos\,\theta_{\mu k}}\right)^2\frac{R_1}{R_0}. \tag{50}$$

As an example, we assume that we probe the sidebands on the 282 nm transition in $^{199}Hg^+$ in a trap with the parameters listed previously. If $\theta_{\mu k}=0$ and $R_1/R_0=0.1$, then the second-order Doppler shift is $\Delta\nu_{D2}/\nu\cong-9\times10^{-18}$. The corresponding Stark shift is $|\Delta\nu_S/\nu|\leqslant 2.5\times10^{-18}$.

In the limit $\Omega\ll\gamma$, a sensitive method to detect excess micromotion monitors the modulation of the ion's fluorescence signal due to the first-order Doppler shift.[22–24] We will call this the ''cross-correlation'' technique because the modulation is correlated to the ac potentials applied to the trap electrodes. For simplicity, we assume that the amplitude of the first-order Doppler shift is much less than the linewidth γ. From Eqs. (15) and (18), the velocity due to excess micromotion is given by

$$\mathbf{V}_\mu(t)=-\frac{1}{2}\sum_{i=x,y}u_{0i}q_i\Omega\,\sin(\Omega t)\hat{u}_i$$

$$-\frac{1}{4}q_xR\alpha\varphi_{\mathrm{ac}}\Omega\,\cos(\Omega t)\hat{x}. \tag{51}$$

In the frame of an ion undergoing excess micromotion, the frequency of the laser is Doppler shifted by $-\mathbf{k}\cdot\mathbf{V}_\mu=\beta\Omega\,\sin(\Omega t+\delta)$, where β and δ are defined in Eqs. (22), (23), and (24). In the low intensity limit, the detected fluorescence rate is thus

$$R_d=R_{\max}\frac{(\frac{1}{2}\gamma)^2}{(\frac{1}{2}\gamma)^2+[\omega_{\mathrm{atom}}-\omega_{\mathrm{laser}}-\beta\Omega\,\sin(\Omega t+\delta)]^2}. \tag{52}$$

We take $\omega_{\mathrm{atom}}-\omega_{\mathrm{laser}}=\gamma/2$, which is a natural choice since this minimizes the temperature of the Doppler-cooled ions and because it maximizes the cross-correlation signal. If $\beta\Omega\ll\gamma$, then

$$\frac{R_d}{R_{\max}}\approx\frac{1}{2}+\frac{\beta\Omega\,\sin(\Omega t+\delta)}{\gamma}\equiv\frac{1}{2}+\frac{\Delta R_d\,\sin(\Omega t+\delta)}{R_{\max}}. \tag{53}$$

Using Eq. (48), we can write the fractional second-order Doppler shift as

$$\frac{\Delta\nu_{D2}}{\nu}\approx-\frac{1}{4}\left(\frac{\gamma}{ck\cos\theta_{\mu k}}\frac{\Delta R_d}{R_{\max}}\right)^2. \tag{54}$$

where, again, $\theta_{\mu k}$ is the angle between $\hat{k}$ and the direction of the excess micromotion. With Eqs. (34) and (48), the corresponding Stark shift can be written as

$$\Delta\nu_S=\sigma_S\frac{1}{2}\left(\frac{m\gamma\,\Omega}{Qk\cos\theta_{\mu k}}\frac{\Delta R_d}{R_{\max}}\right)^2. \tag{55}$$

As an example, we consider $^{199}Hg^+$ ions, using the previously stated trap parameters, and $\gamma=2\pi\cdot 70$ MHz for the 194 nm Doppler-cooling transition. If $\theta_{\mu k}=0$ and $\Delta R_d/R_{\max}=0.1$, then the second-order Doppler shift is $\Delta\nu_{D2}/\nu\cong-5\times10^{-18}$, and the Stark shift of the electric quadrupole transition is $|\Delta\nu_S/\nu|\leqslant 1.5\times10^{-17}$.

As opposed to the first method for sensing micromotion, the cross-correlation technique can determine whether the ac potential applied to electrode 2 is out of phase with that applied to electrode 4 (see Fig. 1). If a deliberately applied static electric field moves the ion to different positions in the trap, the phase of the fluorescence modulation at frequency Ω depends on $\varphi_{\rm ac}$. The atomic velocity is 90° out of phase with the force due to the ac electric field. Thus if $\varphi_{\rm ac}=0$, the phase of the cross-correlation signal jumps by 180° as the average position of the ion crosses the nodal line of the ac field. Also, when the ion is on the nodal line, the signal at frequency Ω vanishes. However, if $\varphi_{\rm ac}\neq 0$, from Eq. (18), the phase of micromotion in the x direction continuously varies as the varies as the average ion position is changed. Furthermore, the amplitude of the micromotion is never zero. This behavior can be used to determine the relative contributions of stray static electric fields and electrode potential phase shifts to the excess micromotion. In general, the effects of $\mathbf{E}_{\rm dc}$ can be eliminated by purposely applying a static field $\mathbf{E}_{\rm applied}=-\mathbf{E}_{\rm dc}$; $\varphi_{\rm ac}$ can be made zero by loading electrodes 2 and 4 with the appropriate reactances.

Still, avoidable effects may confuse the interpretation of the cross-correlation signal. For example, as the ion moves back and forth across a nonuniform laser beam intensity profile, the fluorescence is modulated at frequency Ω, even if $\mathbf{k}\cdot\mathbf{V}_\mu=0$. This modulation is minimized when the ion is at the center of the (symmetric) laser beam, regardless of its average distance from the ac field's nodal position. However, this condition can be detected—the phase of this fluorescence modulation is sensitive to lateral translations of the laser beam, which is not true if the fluorescence modulation is due to the first-order Doppler shift.

It is also important to avoid tuning the laser frequency too close to the atomic frequency. In this case, the fluorescence modulation due to the first-order Doppler shift [Eq. (52)] is deceptively small. This situation, though, is easily checked by detuning the laser frequency farther from atomic resonance to see if the fluorescence modulation amplitude increases.

Finally, to determine that the micromotion is zero in all three dimensions, three laser beams must interact with the ion. These beams must not be coplanar, to ensure sensitivity to micromotion in every direction. Unless the three beams are orthogonal, this technique is not equally sensitive to ion motion in all directions, as illustrated below.

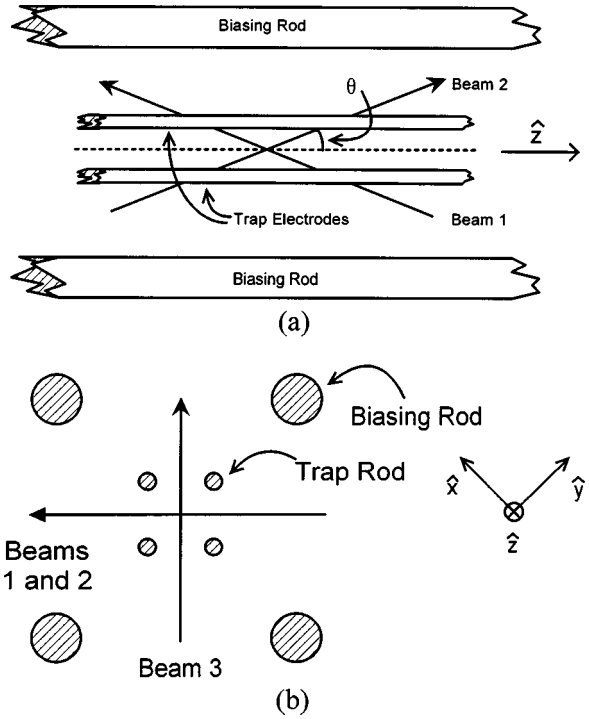

FIG. 3. Experimental setup to observe and minimize micromotion using the cross-correlation technique. The ions are at the intersection of the three laser beams. (a) Top view of the section of the trap in which the ions are located. Beam 3 is not shown. (b) View along the trap axis. For clarity, the origin of the coordinate system has been translated.

V. EXPERIMENTAL DEMONSTRATION OF THE FLUORESCENCE MODULATION TECHNIQUE

Figure 3 illustrates the experimental configuration we use to detect and minimize micromotion of a string of ions in our linear Paul trap, using the cross-correlation technique. In this trap, $\varphi_{\rm ac}=0$ within the experimental resolution. Typically, about ten ions, whose extent is small compared to their distance from the electrodes, are stored in the trap. In this case the fluorescence modulation signals from each ion add in phase. Laser beams 1 and 2 propagate along $\sin\theta[(\hat{x}-\hat{y})/\sqrt{2}]\mp\cos\theta\,\hat{z}$, where $\theta=20°$. Beam 3 propagates along $(\hat{x}+\hat{y})/\sqrt{2}$. The three beams intersect at the ions' position. Static electric potentials are applied to four biasing rods running parallel to the trap electrodes, creating an additional field that is nearly uniform at the site of the ions. When the potentials on the four rods are appropriately summed, the electric fields along the $(\hat{x}\pm\hat{y})/\sqrt{2}$ directions can be separately controlled.

We detect the fluorescence modulation with a START-STOP time-to-amplitude converter (TAC).[25] The TAC generates an analog pulse having a height proportional to the time delay between a START and a STOP pulse. A fluorescence photon, detected by a photomultiplier tube, generates the START pulse. An amplifier discriminator generates a STOP pulse for each negative-going zero crossing of the trap ac potential. The counting rate of fluorescence photons is

typically much less than the frequency of the ac field. Also, the time between photon detections is much greater than the time the TAC takes to reset for the next START pulse. Thus, each detected photon results in an output from the TAC, proportional to the time to the next STOP pulse. This process would be inefficient if the START and STOP trigger sources were reversed, because not every START pulse would be followed by a STOP pulse within a period of the ac electric field. Finally, the height of the output pulse from the TAC is measured by a triggered analog-to-digital converter and binned according to height by a computer, which acts as a multichannel analyzer.[25] A spectrum of the fluorescence intensity as a function of the phase of the ac electric field is typically built up within a few seconds.

The fluorescence modulation signals due to beams 1, 2, and 3 are separately measured, then the static fields are adjusted to minimize the fluorescence modulation for each beam. Since the micromotion is directed along the ac electric field, in general, the direction of the micromotion is not the direction of the ion displacement from the trap axis. For example, in the trap of Figs. 1 and 3, micromotion along $(\hat{x}+\hat{y})/\sqrt{2}$ indicates that the ions are displaced along $(\hat{x}-\hat{y})/\sqrt{2}$, and vice versa. To begin, we compare the cross-correlation signal $\Delta R_d/R_{\max}$ with only beam 1 present to $\Delta R_d/R_{\max}$ with only beam 2 present. The signals due to the two beams will differ if the ions experience micromotion along $\hat{z}$. Such axial micromotion is due to the endcaps, which produce a (small) component of the ac electric field along $\hat{z}$. From symmetry, this axial micromotion should be minimized when the ions are equidistant from the endcaps. A differential potential is applied between the two endcaps to translate the ions along the trap axis until the signals from beams 1 and 2 are nearly equal. Next, the static field along $(\hat{x}+\hat{y})/\sqrt{2}$ is adjusted to move the ions to a position at which $\Delta R_d/R_{\max}$ from beams 1 and 2 are each minimized. Typically, we must iterate these adjustments before $\Delta R_d/R_{\max} \approx 0$ for both beams 1 and 2. Finally, a static field along $(\hat{x}-\hat{y})/\sqrt{2}$ is applied to null the amplitude of the signal from beam 3. After this we check that the signals from beams 1 and 2 have remained negligible. If they have increased, we repeat the entire process until the micromotion is eliminated in all three dimensions.

Figure 4 shows some fluorescence modulation signals collected with the setup shown in Fig. 3, when only beam 1 is present. The laser is tuned near the 194 nm $5d^{10}6s\ ^2S_{1/2} \rightarrow 5d^{10}6p\ ^2P_{1/2}$ transition. Here, $\Omega = 2\pi \cdot 8.6$ MHz, $\omega_x \approx \omega_y \approx 2\pi \cdot 65$ kHz, and $\omega_{\text{laser}} - \omega_{\text{atom}} \cong -\gamma/2$. The micromotion has been nulled in all three dimensions as just described.

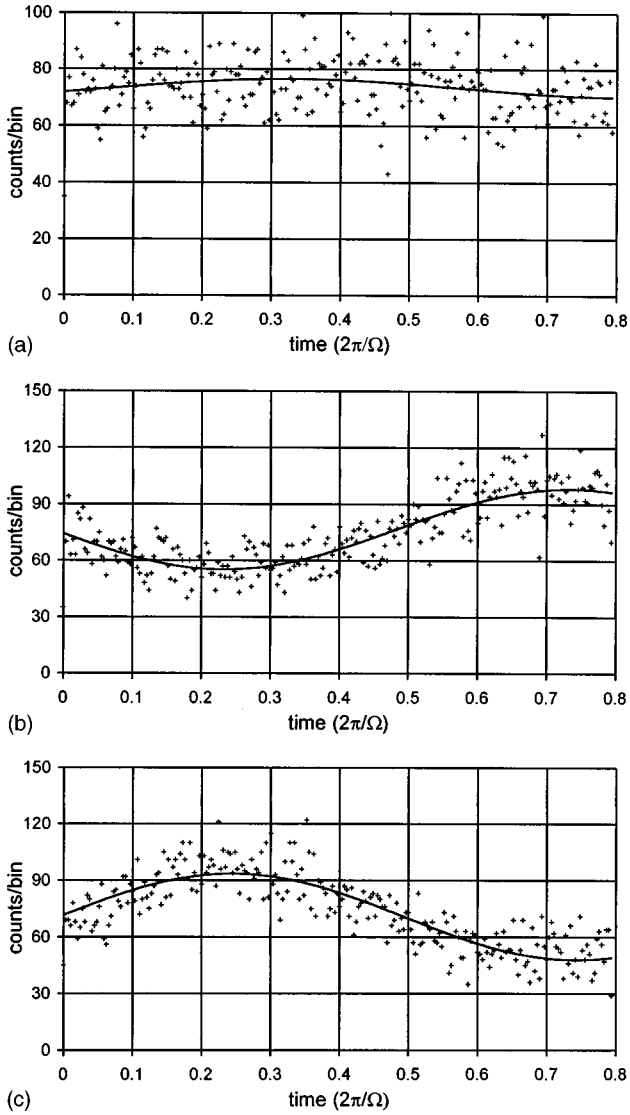

FIG. 4. Experimental fluorescence modulation signals for beam 1 of Fig. 3, using eight ions in the linear trap (points) and fit (solid line). Displacement of the ions from the trap axis along $(\hat{x}+\hat{y})/\sqrt{2}$ is (a) $0.9 \pm 0.3\ \mu$m, (b) $6.7 \pm 0.4\ \mu$m, and (c) $-6.7 \pm 0.4\ \mu$m.

TABLE I. Summary of the sensitivities of various techniques to the fractional second-order Doppler shift and the Stark shift. Formulas are approximations assuming $|a_i| \ll q_i^2 \ll 1$ $(i=x,y)$. Here, $(\Delta\nu_{2D}/\nu)_i$ is the fractional second-order Doppler shift due to motion along direction $\hat{u}_i$, $(\Delta\nu_S)_i$ the Stark shift due to the electric field along direction $\hat{u}_i$, $\mathbf{k}$ the wave vector, and γ the width of the excited transition, m the ion mass, Q the ion charge, Ω the trap drive frequency, ω_i the secular frequency along direction $\hat{u}_i$, and $\theta_{\mu k}$ the angle between the direction of the micromotion and $\mathbf{k}$.

Method	$\Delta\nu_{2D}/\nu$	$\Delta\nu_S$
Directly monitor ion displacement Δu_{0i} along direction $\hat{u}_i$ as ω_i is changed from ω_{i1} to ω_{i2}	$\left(\frac{\Delta\nu_{D2}}{\nu}\right)_i \cong -\frac{1}{2}\left(\frac{\omega_{i2}^2}{\omega_{i1}^2-\omega_{i2}^2}\frac{\Delta u_{0i}\omega_{i1}}{c}\right)^2$	$(\Delta\nu_S)_i \cong \sigma_S\left(\frac{\omega_{i2}^2}{\omega_{i1}^2-\omega_{i2}^2}\frac{m\Delta u_{0i}\omega_{i1}\Omega}{Q}\right)^2$
Measure ratio R_1/R_0 of scattering rates of carrier and first sideband $(\Omega \gg \gamma)$	$\approx -\left(\frac{\Omega}{ck\cos\theta_{\mu k}}\right)^2\frac{R_1}{R_0}$	$2\sigma_S\left(\frac{2m\Omega^2}{Qk\cos\theta_{\mu k}}\right)^2\frac{R_1}{R_0}$
Monitor cross-correlation signal $\Delta R_d/R_{\max}$ due to first-order Doppler shift $(\Omega \ll \gamma)$	$\approx -\frac{1}{4}\left(\frac{\gamma}{ck\cos\theta_{\mu k}}\frac{\Delta R_d}{R_{\max}}\right)^2$	$\frac{1}{2}\sigma_S\left(\frac{m\gamma\Omega}{Qk\cos\theta_{\mu k}}\frac{\Delta R_d}{R_{\max}}\right)^2$

Next, only beam 1 is used as the ions are translated along $(\hat{x}+\hat{y})/\sqrt{2}$ to induce excess micromotion along $(\hat{x}-\hat{y})/\sqrt{2}$. Figure 4(a) shows the cross-correlation signal when the ions are located near the trap axis. The fit to the data gives $\Delta R_d/R_{\max}=0.043\pm0.014$, corresponding to a fractional second-order Doppler shift of $\Delta\nu_{D2}/\nu\cong-(9\pm3)\times10^{-19}$ due to motion along the propagation direction of beam 1. Figures 4(b) and 4(c) are the fluorescence modulation signals when the ions are deliberately shifted by approximately ±6.7 μm along $(\hat{x}+\hat{y})/\sqrt{2}$. For these signals, $|\Delta R_d/R_{\max}|\approx0.3$, corresponding to a second-order Doppler shift of $\Delta\nu_{D2}/\nu\cong-5\times10^{-17}$ due to motion along the propagation direction of beam 1. The Stark shift due to the ac field along the propagation direction of beam 1 is $|\Delta\nu_S/\nu|\leqslant1.0\times10^{-16}$.

The fluorescence modulation signals from all three laser beams can be reduced to the level shown in Fig. 4(a). We consider the case in which the signals from beams 1 and 2 have the same sign. Then from Eq. (54), the fractional second-order Doppler shifts due to excess micromotion is $-(0\pm0.2)\times10^{-18}$ along $\hat{z}$, $-(8\pm2)\times10^{-18}$ along $(\hat{x}-\hat{y})/\sqrt{2}$, and $-(0.9\pm0.3)\times10^{-18}$ along $(\hat{x}+\hat{y})/\sqrt{2}$. These values add to give a total shift of $\Delta\nu_{D2}/\nu\cong-(9\pm2)\times10^{-18}$. Similarly, from Eq. (55), these signals indicate a total Stark shift of $|\Delta\nu_S/\nu|\leqslant(1.9\pm0.4)\times10^{-17}$. These small shifts illustrate this method's effectiveness in reducing micromotion.

To conclude, the micromotion of ions in a Paul trap has several related adverse effects. In high-resolution spectroscopy, the most significant are the second-order Doppler shift and a possible Stark shift due to the ac electric fields. Because these shifts can be substantial, it is critical that micromotion be eliminated in all three dimensions. Table I lists the methods discussed in this article, and the corresponding formulas for determining the second-order Doppler shift and the Stark shift from the relevant signals. The first method monitors the spatial motion of the ions as the pseudopotential is varied, whereas the last two methods monitor the effects of first-order Doppler shift on the atomic line shape. The spatial-monitoring techniques are insensitive to micromotion caused by a phase shift between the ac potentials applied to the trap electrodes. Apart from this, which technique is most sensitive to micromotion depends on the parameters of the trap, laser beams, and atomic transition.

ACKNOWLEDGMENTS

This work was supported by ONR and ARO. The authors thank Dietrich Leibfried, Don Sullivan, Brent Young, and Matt Young for helpful comments on the manuscript.

[1] D. J. Wineland, J. C. Bergquist, J. J. Bollinger, W. M. Itano, D. J. Heinzen, S. L. Gilbert, C. H. Manney, and M. G. Raizen, IEEE Trans. Ultrason. Ferroelectr. Freq. Control **37**, 515 (1990).
[2] J. Prestage, G. J. Dick, and L. Maleki, J. Appl. Phys. **66**, 1013 (1989); R. L. Tjoelker J. D. Prestage, and L. Maleki, in *Fifth Symposium on Frequency Standards and Metrology*, edited by J. C. Bergquist, Woods Hole, MA, Oct. 1995 (World Scientific, Singapore, 1996), p. 33.
[3] M. G. Raizen, J. M. Gilligan, J. C. Bergquist, W. M. Itano, and D. J. Wineland, Phys. Rev. A **45**, 6493 (1992).
[4] P. T. H. Fisk, M. J. Sellars, M. A. Lawn, C. Coles, in *Fifth Symposium on Frequency Standards and Metrology*, edited by J. C. Bergquist, Woods Hole, MA, Oct. 1996 (World Scientific, Singapore, 1996), p. 27.
[5] M. E. Poitzsch, J. C. Bergquist, W. M. Itano, and D. J. Wineland, Rev. Sci. Instrum. **67**, 129 (1996).
[6] H. C. Naegerl, W. Bechter, J. Eschner, F. Schmidt-Kaler, and R. Blatt, Appl. Phys. B **66**, 603 (1998).
[7] H. Walther, Adv. At., Mol., Opt. Phys. **31**, 137 (1993).
[8] W. Paul, Rev. Mod. Phys. **62**, 531 (1990).
[9] L. D. Landau and E. M. Lifshitz, in *Mechanics* (Pergamon, New York, 1976), pp. 93–95.
[10] W. M. Itano, J. C. Bergquist, J. J. Bollinger, and D. J. Wineland, Phys. Scr. **T59**, 106 (1995).
[11] D. J. Wineland, W. M. Itano, J. C. Bergquist, and R. G. Hulet, Phys. Rev. A **36**, 2220 (1987).
[12] A. van Wijngaarden and G. W. F. Drake, Phys. Rev. A **17**, 1366 (1978).
[13] N. Yu, W. Nagourney, and H. Dehmelt, J. Appl. Phys. **69**, 3779 (1991).
[14] R. G. DeVoe, J. Hoffnagle, and R. G. Brewer, Phys. Rev. A **39**, 4362 (1989).
[15] R. Blümel, C. Kappler, W. Quint, and H. Walther, Phys. Rev. A **40**, 808 (1989).
[16] N. Yu, X. Zhao, H. Dehmelt, and W. Nagourney, Phys. Rev. A **50**, 2738 (1994).
[17] D. A. Church and H. G. Dehmelt, J. Appl. Phys. **40**, 3421 (1969).
[18] C. Tamm (unpublished). Talk presented in *Proceedings of the Fifth Symposium on Frequency Standards and Metrology*, edited by C. Bergquist (World Scientific, Singapore, 1996).
[19] H. A. Schuessler and H. S. Lakkaraju, in *Precision Measurement and Fundamental Constants II*, edited by B. N. Taylor and W. D. Phillips, Natl. Bur. Stand. (U.S.), Spec. Publ. 617 (1984), p. 103.
[20] M. Jardino, F. Plumelle, M. Desaintfuscien, and J. L. Duchene, in *Proceedings of 38th Annual Symposium on Frequency Control*, IEEE 84CH2062-8 (IEEE, New York, 1984), p. 431; L. S. Cutler, C. A. Flory, R. P. Giffard, and M. D. McGuire, Appl. Phys. B **39**, 251 (1986).
[21] J. C. Bergquist, Wayne M. Itano, and D. J. Wineland, Phys. Rev. A **36**, 428 (1987).
[22] G. R. Janik, Ph.D. thesis, University of Washington (University Microfilms International, 1984).
[23] F. Diedrich and H. Walther, Phys. Rev. Lett. **58**, 203 (1987).
[24] J. T. Höffges, H. W. Baldauf, T. Eichler, S. R. Helmfrid, and H. Walther, Opt. Commun. **133**, 170 (1997).
[25] W. R. Leo, *Techniques for Nuclear and Particle Physics Experiments*, second revised edition (Springer, Berlin, 1994).